2006

Exchange Coupling and Contribution of Induced Orbital Angular Momentum of Low-Spin Fe^3+ Ions to Magnetic Anisotropy in Cyanide-Bridged Fe2M2 Molecular Magnets: Spin-Polarized Density-Functional Calculations

Stephen Holmes, *University of Missouri-St. Louis*
Kyungwha Park, *Virginia Polytechnic Institute and State University*

Exchange coupling and contribution of induced orbital angular momentum of low-spin Fe^{3+} ions to magnetic anisotropy in cyanide-bridged Fe_2M_2 molecular magnets: Spin-polarized density-functional calculations

Kyungwha Park[1,*] and Stephen M. Holmes[2,†]

[1]*Department of Physics, Virginia Polytechnic Institute and State University, Blacksburg, Virginia 24061-0435, USA*

[2]*Department of Chemistry, University of Kentucky, Lexington, Kentucky 40506-0055, USA*

(Received 13 September 2006; revised manuscript received 3 November 2006; published 28 December 2006)

Electronic structure and intramolecular exchange constants are calculated for three cyanide-bridged molecular magnets, $[Tp^{\star}Fe^{III}(CN)_3M^{II}(DMF)_4]_2(OTf)_2\cdot 2DMF$ (M^{II}=Mn,Co,Ni) (abbreviated as Fe_2Mn_2, Fe_2Co_2, and Fe_2Ni_2) that have been recently synthesized, within a generalized-gradient approximation in spin-polarized density-functional theory (DFT). Here $Tp^{\star}=[C_3(CH_3)_2HN_2]_3BH$, $OTf=O_3SCF_3$, and $DMF=HCON(CH_3)_2$. Due to strong ligand fields present in the $[Tp^{\star}Fe^{III}(CN)_3]^-$ units, the Fe^{3+} ions exhibit a low ground-state spin of $S=1/2$. Our calculations show that the metal ions in the Fe_2Mn_2 molecule interact antiferromagnetically via cyanide ligands, while those in the Fe_2Co_2 and Fe_2Ni_2 molecule interact ferromagnetically. The calculations also suggest that the smallest gaps between the highest occupied molecular orbital (HOMO) and the lowest unoccupied molecular orbital (LUMO) for Fe_2Mn_2, Fe_2Co_2, and Fe_2Ni_2 are 0.12, 0.03, and 0.33 eV. Based on the calculated electronic structures, the second-order magnetic anisotropy is computed including single-electron spin-orbit coupling within a DFT formalism. In comparison to a prototype single-molecule magnet Mn_{12}, the three cyanide-bridged molecular magnets are found to bear substantial transverse magnetic anisotropy that becomes 15%–36% of molecular longitudinal anisotropy. Spin-orbit coupling arising from the low-spin Fe^{3+} and high-spin Co^{2+} ions induces significant orbital angular momentum that contributes to the total magnetic anisotropy of the three cyanide-bridged molecular magnets. The induced orbital angular momentum is 4–8 times those calculated for Mn_{12}. The total magnetic anisotropy present in the three molecular magnets is due to competition between the magnetic anisotropy of the Fe^{3+} and of the M^{2+} ions. In the Fe_2Mn_2 and Fe_2Ni_2 molecules, the anisotropy is primarily due to the Fe^{3+} ions, while in the Fe_2Co_2 molecule, the single-ion anisotropy of the Co^{2+} ions counters the Fe^{3+} contributions. These results are supported by previously reported magnetic measurements.

DOI: 10.1103/PhysRevB.74.224440 PACS number(s): 75.50.Xx, 71.15.Mb, 75.30.Gw, 75.30.Et

I. INTRODUCTION

Over the past decade, single-molecule magnets (SMMs) have drawn considerable attention due to their observation of quantum tunneling of the magnetization and of significant energy barriers to reverse magnetic moments in zero external magnetic field.[1–4] SMMs are soluble, well-defined molecules consisting of several transition metal ions interacting through various surrounding ligands. Some of the metal ions in SMMs possess strong magnetic anisotropy which induces energy barriers for magnetization reversal. For typical SMMs, a substantial separation between different molecules, an order of a few nanometers, prevents individual molecules from interacting through direct or indirect exchange coupling. The first prototype SMM is $[Mn_{12}O_{12}(O_2CCH_3)_{16}(H_2O)_4]$ (abbreviated as Mn_{12}) (Ref. 5) in which the 12 Mn ions are interacting through the oxygen anions via superexchange. Due to the energy barriers, magnetization of SMMs relaxes unusually slowly in response to external fields at low temperatures. Consequently, an out-of-phase component of ac susceptibility depends on the ac frequency as well as magnetic hysteresis occurs even though magnetic ordering has not been observed for SMMs.

The electronic structure and magnetic anisotropy of the prototype oxygen-bridged SMM Mn_{12} (Ref. 5) were first calculated by Pederson and Khanna,[6] within a density-functional theory (DFT) formalism,[7] considering single-electron spin-orbit coupling. The calculated second-order magnetic anisotropy for Mn_{12} was in good agreement with a variety of spectroscopic measurements such as electron paramagnetic resonance (EPR),[2,3,8,9] inelastic neutron scattering,[10–12] and high-frequency magnetic spectroscopy.[13] The DFT calculations on the electronic and magnetic properties of another oxygen-bridged SMM Mn_4 (Ref. 14) also showed good agreement with experiment.[15] However, when higher-order anisotropy terms play an important role or low-energy excited spin multiplets become highly mixed with the ground-state spin multiplets,[16] DFT-calculated second-order magnetic anisotropy barriers tend to be considerably smaller than measured anisotropy barriers. Exchange coupling constants within an individual SMM were calculated for various types of SMMs including Mn_{12} using low-energy collinear or broken-symmetry spin configurations in DFT.[17–21] An approximate exchange-correlation potential used in DFT includes an unphysical interaction of an electron with itself, referred to as a self-interaction.[22] Due to this unphysical interaction, the approximate exchange-correlation potential is less attractive and the gap between occupied and unoccupied orbitals is underestimated.[23,24] As a result, electrons would be more delocalized without self-interaction corrections in a density-functional formalism. Including on-site Coulomb repulsion U in DFT would play the same role as the self-interaction correction. Thus, the exchange constants calculated using DFT without self-interaction corrections or the

parameter U are likely overestimated compared to the experimentally deduced values. Recently, exchange coupling constants for SMMs Mn_{12} and V_{15} have been computed including the parameter U.[25,26] These constants were reported to be about a factor of 2 or 3 less than the DFT values.[17,19] Despite all of these limitations, DFT is one of the most powerful tools for investigating complex systems due to its ability to deal with large systems consisting of a few hundreds of atoms, within a desirable accuracy.

Compared to extensive studies of oxygen-bridged SMMs, there have been, so far, few theoretical and experimental studies on another class of SMMs known as cyanometalates or cyanide-bridged SMMs. The cyanometalates are often constructed using a building block synthetic approach, where discrete molecular precursors are allowed to self-assemble into a common structural archetype. The resulting polynuclear molecules contain metal-(cyanide,CN)-metal units, where cyanide-mediated superexchange interactions electronically couple the metal ions. A judicious choice of transition metal ions allows for the rational construction of a series of structurally related clusters whose electronic, magnetic, and optical properties can be tuned via the metal ions. The first reported example of a cyanide-bridged SMM is $\{[(Me_3tacn)Mo^{III}(CN)_3]_6Mn^{II}\}^{4+}$ cluster[27] in which the magnetic anisotropy arises from the six Mo^{3+} ($S=3/2$) ions. Later other types of cyanide-bridged SMMs were synthesized in a form of $[Mn^{III}(CN)_6]_2[Mn^{II}(tmphen)_2]_3$ [abbreviated as $Mn(III)_2Mn(II)_3$],[28] as well as of $(Mn^{III}Cl)_4\{Re^{II}(triphos)(CN)_3\}_4$ (abbreviated as Mn_4Re_4) in which the four Re^{2+} and four Mn^{2+} ions are at the corners of the cube.[29] In the $Mn(III)_2Mn(II)_3$ and Mn_4Re_4 molecules, the low-spin Mn^{3+} (t_{2g}^4, $S=1$) and Re^{2+} (t_{2g}^5, $S=1/2$) ions were shown to primarily contribute to the total magnetic anisotropy via the Jahn-Teller effect and spin-orbit coupling interactions. In addition to these, linear, square, face-centered-cubic, and simple-cubic cyanide-bridged clusters have been experimentally realized.[30–34] The exchange coupling constants for some of the cyanide-bridged SMMs have been calculated within a collinear spin (broken-symmetry) approximation using DFT by several groups.[35–37] When a $3d$, $4d$, or $5d$ transition metal ion is in an octahedral ligand field, the degeneracy of the d orbitals is partially lifted to form upper doubly degenerate e_g and lower triply degenerate t_{2g} levels. When the degenerate t_{2g} levels are partially occupied except for a half-filling, orbital angular momentum is not quenched even without spin-orbit coupling. In cyanide-bridged SMMs, some metal ions can possess unquenched orbital angular momentum due to partially filled t_{2g} levels caused by strong ligand fields, which leads to nonzero first-order spin-orbit coupling.[38,39] In contrast, in oxygen-bridged SMMs, metal ions have quenched orbital angular momentum due to weak ligand fields so that a second-order spin-orbit coupling effect is expected. Recent theoretical studies on the $Mn(III)_2Mn(II)_3$ molecule suggested that the Mn^{3+} ions (t_{2g}^4) may have unquenched orbital angular momentum and that the total magnetic anisotropy and other magnetic properties can be understood by considering both unquenched orbital angular momentum and a crystal field in the spin Hamiltonian.[38,39] The parameter values in the Hamiltonian were obtained by fitting to experimental data. However, there have been, so far, to our best knowledge, no reports in first-principles studies of the magnetic anisotropy of cyanide-bridged SMMs. Our DFT studies will provide insight into magnetic anisotropy barrier and magnetic quantum tunneling rates for the cyanide-bridged SMMs, without fitting to experimental data, as well as insight into electronic structures of the SMMs in comparison to those of oxygen-bridged SMMs.

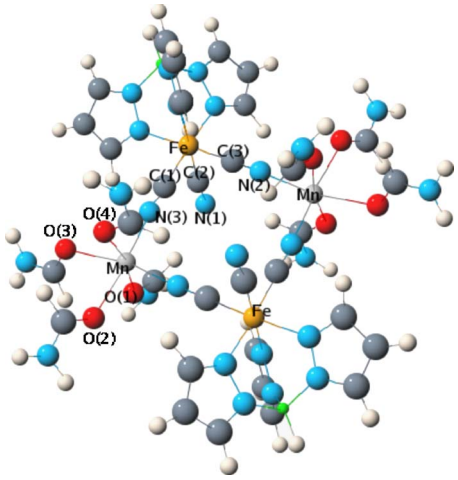

FIG. 1. (Color online) Geometry of a simplified form of a single $[Fe_2Mn_2]^{2+}$ molecule. The original chemical formula is $\{[(Tp^{\star})Fe(CN)_3M(DMF)_4]_2\}^{2+}$. When the Mn ions are replaced by Co or Ni ions, this geometry becomes $[Fe_2Co_2]^{2+}$ or $[Fe_2Ni_2]^{2+}$. Each Fe ion is surrounded by $Tp^{\star}(CN)_3$, while each Mn (Co or Ni) ion is surrounded by $(NC)_2$ and $(DMF)_4$.

Herein, we discuss, within a DFT formalism, calculations of the magnetic anisotropy and of exchange coupling for a series of cyanide-bridged molecules recently synthesized,[32] $\{[(Tp^{*})Fe^{III}(CN)_3M^{II}(DMF)_4]_2(OTf)_2\}\cdot 2DMF$ where M^{II} =Mn, Co, and Ni. In our calculations, we do not include either the on-site Coulomb repulsion U or the self-interaction correction. Implementation of the parameter U into DFT may reduce the values of the exchange constants by up to a factor of 3. However, there are no evidences that the parameter U would significantly improve the magnetic anisotropy of SMMs. The simplified structures of the cyanide-bridged molecules are illustrated in Fig. 1. Henceforth, these molecules are abbreviated as Fe_2Mn_2, Fe_2Co_2, and Fe_2Ni_2 unless specified otherwise. The ligands $Tp^{*}=[C_3(CH_3)_2HN_2]_3BH$ and $OTf=O_3SCF_3$ have net charges of -1, and DMF $=HCON(CH_3)_2$ is neutral. For Fe_2Co_2 and Fe_2Ni_2, an out-of-phase component of the ac susceptibility was frequency dependent near 1.8 K,[32] suggesting that both molecules exhibit slow relaxation of the magnetization. However, for Fe_2Mn_2, frequency-dependent behavior has not been observed above 1.8 K.[32] The nominal occupations of $3d$ orbitals and resulting spin and orbital angular momenta of the Fe^{3+}, Mn^{2+}, Co^{2+}, and Ni^{2+} ions in the cyanide-based SMMs are shown in Table I. The methods and specific cluster geometries used for our calculations are described in Sec. II. Calculations of the electronic structure and exchange coupling constants are presented in Sec. III. The calculated exchange constants in-

TABLE I. Nominal occupation numbers $n(e_g)$ and $n(t_{2g})$ of $3d$ orbitals and nominal spin S and orbital angular momenta L of the Fe^{3+}, Mn^{2+}, Co^{2+}, and Ni^{2+} ions in the three cyanide-bridged single-molecule magnets illustrated in Fig. 1.

	Fe^{3+}	Mn^{2+}	Co^{2+}	Ni^{2+}
$n(e_g)$	0	2	2	2
$n(t_{2g})$	5	3	5	6
S	1/2	5/2	3/2	1
L	1	0	1	0

dicate that the metal ions in the Fe_2Mn_2 molecule are antiferromagnetically coupled, while those in the Fe_2Co_2 and Fe_2Ni_2 molecules are ferromagnetically coupled. Magnetic anisotropy is discussed in Sec. IV. Given the ligand fields around the Fe^{3+} ions in the three cyanide-bridged compounds, the Fe^{3+} (t_{2g}^5) ions have a low ground-state spin of $S=1/2$, due to a large separation between the t_{2g} and e_g levels, compared to the Coulomb repulsion between electrons. In this case, we find that significant orbital angular momentum is induced via spin-orbit coupling which arises from the t_{2g} levels of the Fe ions and subsequently contributes to the total magnetic anisotropy. The induced orbital angular momentum is by a factor of 4–8 greater than that for Mn_{12}. Our calculations reveal that the calculated transverse magnetic anisotropy is 15%–36% of the longitudinal anisotropy, which greatly enhances the magnetic quantum tunneling compared to Mn_{12}. At last, the conclusion is made in Sec. V.

II. DFT CALCULATIONS

Crystals of Fe_2Ni_2 (Fe_2Mn_2 and Fe_2Co_2) molecules crystallize in the monoclinic space group with four (two) molecules per unit cell.[32] Different molecules are well separated from one another. For example, the shortest distance between neighboring Fe ions of adjacent molecules is 9.8–9.9 Å. For all calculations on the Fe_2Ni_2, Fe_2Mn_2, and Fe_2Co_2 molecules, we consider truncated clusters, $\{[(Tp^*)Fe(CN)_3M(DMF)_4]_2\}^{2+}$, because O$Tf$ anions do not convey exchange interactions. We treat the clusters in the gas phase in order to reduce computational costs, while physical and chemical features are retained. We further simplify the molecule by substitution of H for CH_3 in the ligands DMF and Tp^*. Since the original molecule is neutral in charge, the fragment $[(Tp^*)Fe(CN)_3M(DMF)_4]$ will have a net total charge of +1. After this pruning, the total number of the atoms within a molecule sums up to 116. Henceforth, this simplified form of the molecule is used in our calculations and abbreviated as $[Fe_2M_2]^{2+}$ (M=Mn,Co,Ni) (Fig. 1). The geometry of $[Fe_2M_2]^{2+}$ is taken from x-ray crystallographic data[32] with corrections in the bond lengths between hydrogen atoms and nearest neighboring nonhydrogen atoms to standard values. These corrections are necessary because x-ray structural analyses often cannot find hydrogen atoms and utilize a fixed distance and a model during refinement of the data. The geometry is not further optimized in order to prevent the cationic entity from being shrunk in size upon relaxation using DFT. Our study confirms that the relaxation of the cationic molecules reduces the distance between neighboring metal sites such that the exchange coupling constants increase by at least an order of magnitude. This would be avoided by more computationally expensive periodic-structure calculations including anions OTf in a unit cell.

TABLE II. The Gaussian basis sets used in the calculation for the three cyanide-based molecular magnets. The minimum and maximum exponents $\alpha_{\min}$ and $\alpha_{\max}$ (in units of $1/a_B^2$) of the bare Gaussian functions, the number of the bare Gaussians N_{bare}, and the number of contracted s, p, and d basis functions, N_s, N_p, and N_d.

	$\alpha_{\min}$	$\alpha_{\max}$	N_{bare}	N_s	N_p	N_d
Mn	0.0416	3.58×10^6	20	7	5	5
Fe	0.0452	3.87×10^6	20	7	5	5
Co	0.0483	4.21×10^6	20	7	5	5
Ni	0.0508	4.45×10^6	20	7	5	5
B	0.0548	1.72×10^4	12	5	4	4
C	0.0772	2.22×10^4	12	5	4	4
N	0.0941	5.17×10^4	13	5	4	4
O	0.1049	6.12×10^4	13	5	4	4
H	0.0745	7.78×10^1	6	4	4	2

Our DFT calculations are performed with spin-polarized all-electron Gaussian-orbital-based Naval Research Laboratory Molecular Orbital Library (NRLMOL)[40] which is ideal for studying isolated molecules. In NRLMOL, the Kohn-Sham orbitals $\Psi_i(\vec{r})$ are expressed as

$$\Psi_i(\vec{r}) = \sum_\sigma \left(\sum_{k=1}^{N_A} \sum_{j=1}^{N_k} C_{j,i\sigma}^k \phi_j^k(\vec{r} - \vec{R}_k) \right) \chi_\sigma, \tag{1}$$

where χ_σ is a spinor, $C_{j,i\sigma}^k$ are coefficients to be determined, and ϕ_j^k is the jth basis function of the kth atom located at $\vec{R}_k$. N_A is the number of atoms and N_k is the total number of basis functions that depends on the type of atoms. As an exchange-correlation potential, the Perdew-Burke-Ernzerhof (PBE) generalized-gradient approximation (GGA)[41] is used unless specified otherwise. The Gaussian basis sets[42] used in the calculation are given in Table II.

III. ELECTRONIC STRUCTURE AND EXCHANGE COUPLING

For a particular collinear spin configuration (Ising-like spin configuration) of $[Fe_2M_2]^{2+}$, a magnetic moment is computed by assigning a sphere around the position of an atom. As shown in Table III, the Fe^{3+} ions surrounded by the given ligands have a low ground-state spin of $S=1/2$ instead of a high spin of $S=5/2$, due to strong ligand fields. However, for the Mn^{2+}, Co^{2+}, and Ni^{2+} ions, the ligand fields are not so strong that high-spin states are preferred for the ground state. (Refer to Table I for nominal spin and orbital angular momenta for the metal ions.) This feature is corroborated in the calculated projected density of states (DOS) onto

TABLE III. Calculated magnetic moments of selected atoms (Fig. 1) in units of μ_B. The moments are not integer values since they were calculated by enclosing a sphere around each atom in the three molecules.

	$[Fe_2Mn_2]^{2+}$	$[Fe_2Co_2]^{2+}$	$[Fe_2Ni_2]^{2+}$
Ground-state spin	$S=4$	$S=4$	$S=3$
Fe^{3+}	0.7802	−0.8902	−0.8960
Mn^{2+}, Co^{2+}, Ni^{2+}	−4.3645	−2.6542	−1.6191
C(1)	−0.0428	0.0128	0.0131
C(2)	−0.0181	0.0173	0.0207
C(3)	−0.0424	0.0120	0.0145
N(1)	0.0271	−0.0164	−0.0306
N(2)	0.0017	−0.0631	−0.0660
N(3)	0.0007	−0.0664	−0.0562
O(1)	−0.0265	−0.0534	−0.0570
O(2)	−0.0168	−0.0388	−0.0416
O(3)	−0.0183	−0.0402	−0.0478
O(4)	−0.0293	−0.0486	−0.0547

the majority and minority Fe, Mn, Co, and Ni 3*d* orbitals as illustrated in Figs. 2–4. For instance, for $[Fe_2Mn_2]^{2+}$, in the $S=4$ ferrimagnetic spin configuration, the magnetic moments of the Fe^{3+} ions ($S=1/2$) are antiparallel to those of the Mn^{2+} ions ($S=5/2$). Thus the calculated projected DOS onto the *minority* Fe 3*d* orbitals showed a large HOMO-LUMO gap between the occupied t_{2g} and unoccupied e_g levels (Fig. 2). On the other hand, the projected DOS onto the *majority* Mn 3*d* orbitals showed a much smaller gap between the occupied t_{2g} and e_g levels (Fig. 2). Notice that in $[Fe_2Co_2]^{2+}$ the three

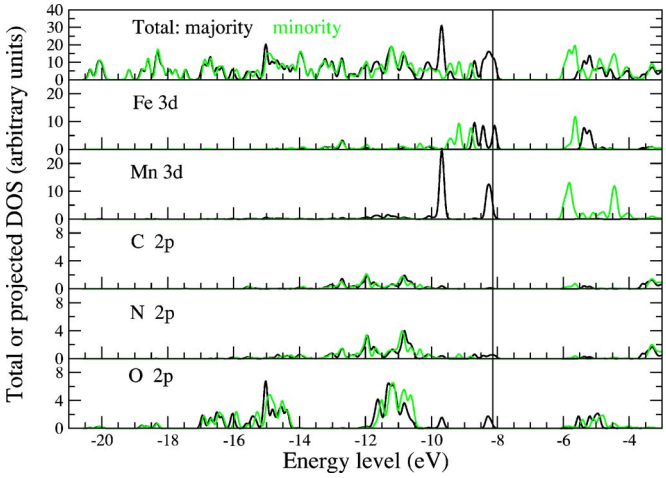

FIG. 2. (Color online) Total density of states (DOS) and projected density of states onto orbitals of specific atoms for majority (black) and minority (green or gray) spin in the $S=4$ ferrimagnetic spin configuration of a single $[Fe_2Mn_2]^{2+}$ molecule. The vertical line indicates the Fermi level. The total density of states has a different scale from the projected density of states onto Fe 3*d* and Mn 3*d* orbitals. Notice that for the Fe 3*d* orbitals, the t_{2g} levels are well separated from the e_g levels and that the t_{2g} levels are clearly split into three near the Fermi level.

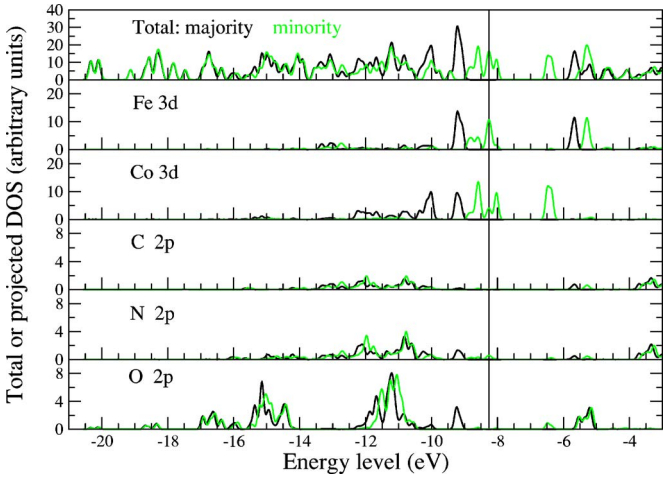

FIG. 3. (Color online) Total and projected density of states onto orbitals of specific atoms for majority (black) and minority (green or gray) spin in the $S=4$ ferromagnetic spin configuration of a single $[Fe_2Co_2]^{2+}$ molecule. The vertical line indicates the Fermi level. Compared to $[Fe_2Mn_2]^{2+}$ and $[Fe_2Ni_2]^{2+}$, the three t_{2g} levels of the Fe ions for majority spin are not well separated. The smallest minority HOMO-LUMO gap is 0.03 eV.

t_{2g} levels of the Fe ions are not as well split as those in $[Fe_2Mn_2]^{2+}$ and $[Fe_2Ni_2]^{2+}$. Most of the spin density is localized on metal sites but some spin density is spread onto neighboring O, C, and N atoms (that are marked in Fig. 1) as shown in Table III and Figs. 2–4.

To determine the ground states for the three molecules, $[Fe_2M_2]^{2+}$ ($M=$Mn, Co, Ni), we consider ferromagnetic and ferrimagnetic collinear (broken-symmetry) spin configurations and calculate their energies self-consistently with magnetic moments fixed in DFT. For $[Fe_2Mn_2]^{2+}$ we find that the ferrimagnetic spin configuration is more stable so that the ground state has an effective total spin of $S=4$. For $[Fe_2Co_2]^{2+}$ and $[Fe_2Ni_2]^{2+}$ the ferromagnetic spin configura-

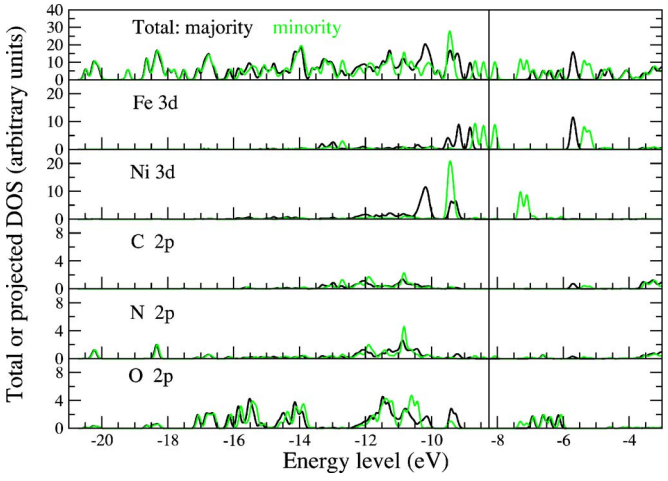

FIG. 4. (Color online) Total density of states and projected density of states onto orbitals of specific atoms for majority (black) and minority (green or gray) spin in the $S=3$ ferromagnetic spin configuration of a single $[Fe_2Ni_2]^{2+}$ molecule. The vertical line indicates the Fermi level.

tion is more stable so that the ground state has, respectively, a total spin of $S=4$ and $S=3$. The DFT results on $[Fe_2Mn_2]^{2+}$ and $[Fe_2Ni_2]^{2+}$ agree with the experimental values deduced from magnetic susceptibility measurements,[32] while the experimental data on $[Fe_2Co_2]^{2+}$ favor a ferrimagnetic spin configuration as a ground state. It is not uncommon to have a discrepancy between experiment and DFT regarding a ground-state spin. It has been reported that a DFT calculation of SMM Ni_4 produced an $S=0$ antiferromagnteic ground state,[43] although experimental data suggested an $S=4$ ferromagnetic ground state.[44] In DFT, it is assumed that a single Slater's determinant is a good approximation to a ground state. However, when an antiferromagnetic or ferrimagnetic spin configuration is expected to be a ground state, more than one Slater's determinant can significantly contribute to the ground state. As a result, it would be difficult for DFT to provide a true ground state and more advanced theories such as configuration interactions (CI) need to be utilized. Those advanced approaches are, so far, limited to much smaller molecules than the molecules of interest. On the experimental front, further spectroscopic studies such as using high-field EPR techniques will elucidate the ground-state properties.

We examine the energy gaps between the HOMO and LUMO for the three molecules using the PBE-GGA (Ref. 41) as an exchange-correlation potential. The calculated smallest HOMO-LUMO gaps are, respectively, 0.12, 0.03, and 0.33 eV for $[Fe_2M_2]^{2+}$ (M=Mn,Co,Ni). The gap for $[Fe_2Co_2]^{2+}$ is particularly very small compared to that for the SMM Mn_{12}, 0.44 eV. As shown in Fig. 3, for $[Fe_2Co_2]^{2+}$, the $3d$ orbitals of the Fe ions are highly hybridized with those of the Co ions, which is not the case for $[Fe_2Mn_2]^{2+}$ and $[Fe_2Ni_2]^{2+}$. This may cause the very small HOMO-LUMO gap for $[Fe_2Co_2]^{2+}$. As a comparison, the HOMO-LUMO gaps are also calculated using a different exchange-correlation potential such as Perdew-Wang local spin density approximation (PW91-LSDA).[45] For $[Fe_2Mn_2]^{2+}$ the gap is reduced to 0.03 eV, while for $[Fe_2Co_2]^{2+}$ and $[Fe_2Ni_2]^{2+}$ the gaps are not found. The ground-state spin configurations are preserved within the PW91-LSDA for all of the three molecules. For Mn_{12} the smallest HOMO-LUMO gap was reduced from 0.44 eV to 0.34 eV when an exchange-correlation potential changed from PBE-GGA to PW91-LSDA.

As illustrated in Fig. 5, the separation between Fe and (M=Mn,Co,Ni) ions within one molecule is in the range of 5.1–5.26 Å, while the separation between the same kind of metal ions is in the range of 7.0–7.7 Å. The Fe and M ions interact with one another via the cyanide ligands. Consequently, only the exchange interactions between different types of metal ions are included in our calculations. The following exchange spin Hamiltonian is used:

$$\mathcal{H}_{ex} = J(\vec{S}_1 \cdot \vec{S}_2 + \vec{S}_2 \cdot \vec{S}_3 + \vec{S}_3 \cdot \vec{S}_4 + \vec{S}_4 \cdot \vec{S}_1), \qquad (2)$$

where $\vec{S}_i$ is the spin vector operator of the ith metal-ion site and the numbering of the four sites is shown in Fig. 5. Here $J>0$ indicates an antiferromagnetic coupling, while $J<0$ means a ferromagnetic coupling. Notice that in exchange

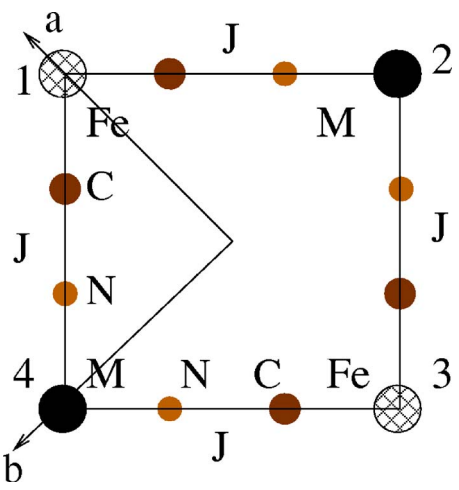

FIG. 5. (Color online) A schematic diagram of a magnetic core of $[Fe_2M_2]^{2+}$ (M=Mn,Co,Ni). The separation between Fe and M is in the range of 5.10–5.25 Å, while the separation between two Fe ions or two M ions is in the range of 7.0–7.7 Å. The Fe ions interact with the M ions via the cyanide ligands in between. Thus, only the exchange interaction J between a Fe ion and an M ion is included in our calculations. The magnetic easy axis is indicated in terms of polar θ and azimuthal angles ϕ in Table IV. The a and b axes are indicated and the c axis comes out of the page.

Hamiltonian, Eq. (2), the definition of J differs from that used in some other groups. The sign of J is opposite and the magnitude of J differs by a factor of 2. The exchange coupling J between metal ions within a molecule is calculated from the energy difference between ferromagnetic and ferrimagnetic spin configurations. The calculated J values are shown in Table IV in comparison to experimental values deduced from the magnetic susceptibility measurements. The magnitude of J increases as the metal ions are replaced by from Mn to Ni. This is partially due to a decrease in the distance between the Fe ion and the other type of metal ion. It is known that the bond angles between the metal ions and the surrounding anions also affect $|J|$. The calculated $|J|$ values are much smaller than those for Mn_{12} (Ref. 46) as shown in Table IV. These calculated $|J|$ values are upper bounds due to considerable electron delocalization caused by the absence of self-interaction corrections in DFT. In the case of $[Fe_2Co_2]^{2+}$, the calculation suggests that the two different spin configurations are very close in energy, which leads to a very small absolute value of J. The sign of the calculated J value is the opposite to the experimental value.

IV. MAGNETIC PROPERTIES

In the three cyanide-bridged compounds, each metal ion is in a slightly distorted octahedral environment as shown in Fig. 1 and as indicated in Table V, which induces anisotropic spin-orbit coupling within a molecule. This anisotropic spin-orbit coupling contributes to nonzero values of the second-order magnetic anisotropy parameters. In this work, we discuss the following three nonrelativistic components out of a general form of the spin-orbit interaction, such as spin-

TABLE IV. The calculated ground-state spin, smallest HOMO-LUMO gap, exchange coupling constant, polar and azimuthal angles (θ and ϕ) of the magnetic easy axis (a and b axes are shown in Fig. 5), longitudinal and transverse magnetic anisotropy parameters D and E, magnetic anisotropy barrier (MAB) calculated using the three methods, and the expectation value of spin-orbit-coupling induced orbital angular momentum $\langle L\rangle$ for three different molecules, $[Fe_2Mn_2]^{2+}$, $[Fe_2Co_2]^{2+}$, and $[Fe_2Ni_2]^{2+}$, in comparison to the SMM Mn_{12}. The numbers in the parentheses are experimental values (Ref. 32). The two values in the MAB are obtained from the first and third methods that are discussed in the text.

	$[Fe_2Mn_2]^{2+}$	$[Fe_2Co_2]^{2+}$	$[Fe_2Ni_2]^{2+}$	Mn_{12}
Ground-state spin	$S=4$ ($S=4$)	$S=4$ ($S=2$)	$S=3$ ($S=3$)	$S=10$ ($S=10$)
HOMO-LUMO gap (eV)	Majority, 0.12	Minority, 0.03	Minority, 0.33	Majority, 0.44 (Ref. 6)
Exchange constant J (K)	18 (6)	−6 (29)	−63 (−15)	140, 117, 7.2, 2.4 (Ref. 46)
θ (easy axis, $\hat{c}$)	66°	49°	66°	0°
ϕ (easy axis, $\hat{a}$)	−6°	−18°	−1.2°	N/A
D (K)	−1.57	−0.50	−2.4	−0.534
E (K)	0.2	0.06	0.5	0
MAB (K)	26, 24 (0)	8.3, 8.7 (18)	23, 20 (52)	53.4, 52
$(\lvert D\rvert-\lvert E\rvert)S^2$ (K)	22	7.0	17.1	53.4
$\langle L\rangle_{\max}$	0.26	0.38	0.45	0.078
$\Delta L=\langle L\rangle_{\max}-\langle L\rangle_{\min}$	0.20	0.11	0.21	0.064

(own) orbit, $\mathcal{H}_{\mathrm{SO}}$, spin-other orbit, $\mathcal{H}_{\mathrm{SOO}}$, and electron-electron spin-orbit coupling terms, $\mathcal{H}_{\mathrm{EESO}}$,[47]

$$\mathcal{H}_{\mathrm{SO}}=-\frac{i}{2c^2}\sum_i\sum_\nu\frac{Z_\nu}{|\vec{r}_i-\vec{R}_\nu|^3}\vec{s}_i\cdot[(\vec{r}_i-\vec{R}_\nu)\times\vec{\nabla}_i], \quad (3)$$

$$\mathcal{H}_{\mathrm{SOO}}=-\frac{i}{2c^2}\sum_i\sum_{j(\neq i)}\frac{1}{|\vec{r}_i-\vec{r}_j|^3}\vec{s}_i\cdot[(\vec{r}_i-\vec{r}_j)\times\vec{\nabla}_j], \quad (4)$$

$$\mathcal{H}_{\mathrm{EESO}}=-\frac{i}{2c^2}\sum_i\sum_{j(\neq i)}\frac{1}{|\vec{r}_i-\vec{r}_j|^3}\vec{s}_i\cdot[(\vec{r}_i-\vec{r}_j)\times\vec{\nabla}_i], \quad (5)$$

where $\vec{s}_i$ is the spin-vector operator of the ith electron, c is the speed of light, and the summation for $i(\nu)$ runs over all electrons located at $\vec{r}_i$ (all nuclei located at $\vec{R}_\nu$ with charge Z_ν). Following the method discussed in Refs. 6 and 48, we consider a nonrelativistic form of the spin-orbit interaction containing spin- (own) orbit coupling $\mathcal{H}_{\mathrm{SO}}$ and electron-electron spin-orbit coupling terms $\mathcal{H}_{\mathrm{EESO}}$ only. Thus, our calculations deal with the interactions between the spin of the ith moving electron and the orbital angular momentum of the ith electron induced by the rest of the electrons and all nuclei treated as stationary and spinless particles in the frame of the ith moving electron. The spin-other orbit terms that are the interactions between the spin of the ith moving electron and the orbital angular momentum of the jth electron are not included in our calculations.

To calculate the magnetic anisotropy parameters for $[Fe_2M_2]^{2+}$ (M=Mn, Co, and Ni), we consider the following single-electron spin-orbit-coupling operator,[6] $\mathcal{H}_{\mathrm{SO}}^{1-el}$,

$$\mathcal{H}_{\mathrm{SO}}^{1-\mathrm{el}}=-\frac{i}{2c^2}\vec{s}\cdot[\vec{\nabla}\Phi_{\mathrm{KS}}(\vec{r})\times\vec{\nabla}], \quad (6)$$

where $\vec{s}$ is a spin vector of an electron and $\Phi_{\mathrm{KS}}(\vec{r})$ is the effective Kohn-Sham potential which includes the interactions between electrons and nuclei and electron-electron interactions in terms of an exchange-correlation potential. The spin-orbit-coupling operator, $\mathcal{H}_{\mathrm{SO}}^{1-\mathrm{el}}$, is treated perturbatively[6] with the calculated Kohn-Sham orbitals and orbital energies. In the energy shift caused by Eq. (6), spatial degrees of freedom are integrated out. Then the following effective single-spin Hamiltonian, $\mathcal{H}_{an}$, is obtained,

$$\mathcal{H}_{an}=DS_z^2+E(S_x^2-S_y^2), \quad (7)$$

where D and E are longitudinal and transverse magnetic anisotropy parameters, and S_z is the z component of the total spin operator. When D is negative, the easy axis is along the z axis. For simplicity, we do not take into account higher-order terms in the magnetic anisotropy. For $D<0$, a second-order magnetic anisotropy barrier can be calculated by (i) an exact diagonalization of $\mathcal{H}_{an}$ or by (ii) a classical treatment of the components of a spin vector in Eq. (7). In the latter (ii), the minimum energy barrier reaches $(|D|-|E|)S^2$, where S is the magnitude of a total spin vector $\vec{S}$. In addition, (iii) the barrier can be obtained as follows.[6] One can exactly diagonalize the total Hamiltonian including the spin-orbit-coupling Hamiltonian, Eq. (6), whose matrix elements are $\langle\phi_j^k\chi_\sigma|(\mathcal{H}_{\mathrm{KS}}+\mathcal{H}_{\mathrm{SO}}^{1-\mathrm{el}})|\phi_l^m\chi_{\sigma'}\rangle$, where $\mathcal{H}_{\mathrm{KS}}$ is the Kohn-Sham Hamiltonian and ϕ_j^k and ϕ_l^m are spatial basis functions shown in Eq. (1). Here only occupied and unoccupied orbitals within a certain energy window are considered. Then one explores how the sum of the eigenvalues over all occupied orbitals within the energy window varies with rotations of the electron spin vector, finding the maximum and minimum values in the sum. The calculated barrier using the three different methods, (i), (ii), and (iii), agree with one another in the range of a few Kelvins when the $|E|$ value is much smaller than the $|D|$ value. If Fe^{3+} (t_{2g}^5) and Co^{2+} ($t_{2g}^5e_g^2$) ions are in a perfect octahedral environment, an expectation value of the orbital angular momentum, $\langle\vec{L}\rangle$, does not vanish even

TABLE V. Bond lengths (in units of Å) between metal ions and their nearest neighboring anions and bond angles (in units of degree) for the three cyanide-bridged molecular magnets. Here M can be Mn, Co, or Ni. The local environment around the Fe ions has much lower symmetry than that around the M ions. Some of the anions are marked in Fig. 1.

	$[Fe_2Mn_2]^{2+}$	$[Fe_2Co_2]^{2+}$	$[Fe_2Ni_2]^{2+}$
M-O(1)	2.193	2.082	2.053
M-O(2)	2.179	2.128	2.079
M-O(3)	2.194	2.088	2.063
M-O(4)	2.163	2.113	2.074
M-N(2)	2.178	2.082	2.039
M-N(3)	2.195	2.077	2.032
O(1)-M-O(2)	89.6	88.5	86.8
O(1)-M-O(3)	85.3	85.9	86.2
O(1)-M-N(2)	92.9	92.6	92.5
O(1)-M-N(3)	89.8	91.5	92.2
O(2)-M-O(3)	85.8	87.9	88.7
O(2)-M-O(4)	90.6	89.9	90.4
O(2)-M-N(2)	87.7	87.8	87.5
O(3)-M-O(4)	91.8	88.0	87.5
O(3)-M-N(3)	92.7	92.1	91.4
O(4)-M-N(2)	90.0	93.3	93.6
O(4)-M-N(3)	89.8	90.1	90.6
N(2)-M-N(3)	93.8	92.2	92.4
Fe-N(4)	1.995	1.993	1.992
Fe-N(5)	1.973	1.987	1.988
Fe-N(6)	2.012	2.013	2.010
Fe-C(1)	1.913	1.920	1.927
Fe-C(2)	1.938	1.922	1.927
Fe-C(3)	1.916	1.916	1.920

without spin-orbit coupling. Thus the first-order spin-order coupling would be expected. The Jahn-Teller distortion around the ions can provide purely orbital anisotropy terms such as $D_{\alpha\beta}L_\alpha L_\beta$, where $D_{\alpha\beta}$ is a parameter tensor and L_α is the α component of the orbital angular momentum. However, in the three molecular magnets of interest, the splitting among the t_{2g} levels of the Fe and Co ions could be significant, due to low-symmetry structures shown in Table V. The quantitative amount of the calculated level splitting will be discussed later in this section. If the level splitting is large, the orbital angular momentum would be at least partially quenched or completely quenched. In this study, we do *not* take into account the effects of unquenched orbital angular momentum (without spin-orbit coupling) and of $D_{\alpha\beta}L_\alpha L_\beta$ terms on the magnetic anisotropy.

Our calculations show that the three molecular magnets are easy-axis systems. With the coordinates illustrated in Fig. 5, the magnetic easy axes are indicated in Table IV in terms of polar θ and azimuthal angles ϕ (the angle between the magnetic easy axis and the a axis). For all the three molecular magnets the values of θ are between 0 and 90°. So the magnetic easy axes are not parallel nor perpendicular to the plane constructed from the four metal ions within a molecule. The azimuthal angle ϕ of the magnetic easy axis for $[Fe_2Co_2]^{2+}$ is quite large compared to those for $[Fe_2Mn_2]^{2+}$ and $[Fe_2Ni_2]^{2+}$. This is because for $[Fe_2Co_2]^{2+}$ both the Fe and Co ions contribute to the magnetic anisotropy, while for the other two molecules the Fe ions mainly contribute to the magnetic anisotropy. As shown in Table IV, the calculated $|E|$ values are approximately 15%–36% of the calculated $|D|$ values due to low symmetry. This large ratio of $|E|$ to $|D|$ contributes to an increase of the rate of magnetic quantum tunneling by several orders of magnitude, compared to highly symmetric SMMs. For a comparison, the calculated magnetic anisotropy barriers using the first and third methods are given in Table IV, as well as the calculated $(|D|-|E|)S^2$ values. Because of the substantial E values, the barrier obtained from $(|D|-|E|)S^2$ is fairly lower than those from the first and third methods. Now we draw attention to two interesting features found in the current theoretical study of the magnetic anisotropy for these molecular magnets. First, our calculations show that the $[Fe_2Mn_2]^{2+}$ and $[Fe_2Ni_2]^{2+}$ molecules possess substantial magnetic anisotropy barriers, although the Jahn-Teller effect is not expected around the Mn^{2+} $(t_{2g}^3e_g^2)$ and Ni^{2+} $(t_{2g}^6e_g^2)$ ions because there is no orbital degeneracy in their ground states. Second, despite the presence of the Jahn-Teller effect around Co^{2+} $(t_{2g}^5e_g^2)$ ions, the calculated magnetic anisotropy barrier of $[Fe_2Co_2]^{2+}$ is much lower than those of $[Fe_2Mn_2]^{2+}$ and $[Fe_2Ni_2]^{2+}$.

As shown in Table V, the bond lengths between metal ions and their nearest neighboring anions indicate much lower symmetry for the environment around the Fe ions than that around the Mn, Co, and Ni ions. Among the local environment around the Mn, Co, and Ni ions, the bond lengths between the Co ions and the neighboring anions are slightly lower symmetric but not as obvious as the case of the Fe ions. For example, the largest difference between the bond lengths is 0.032, 0.051, and 0.047 Å for the Mn, Co, and Ni ions. The deviation of the bond angles from 90°, as shown in Table V, is comparable among the Mn, Co, and Ni ions. Although the Jahn-Teller effect is not expected for the Mn^{2+} and Ni^{2+} ions, there exist apparent distortions of the local environment around these ions. This could be ascribed to accommodation of the distortion caused by the neighboring Fe ions. The apparent distortions of the local environment of the Mn and Ni ions, however, do not lead to the magnetic anisotropy when they are coupled to spin-orbit coupling interactions. Thus, the Mn and Ni ions do not significantly contribute to the total magnetic anisotropy of the molecular magnets. Refer to Table VI. A geometric distortion itself cannot be directly translated into the magnetic anisotropy without including spin-orbit coupling interactions.

In $[Fe_2Mn_2]^{2+}$, since Mn^{2+} ions do not contribute to the magnetic anisotropy due to the reason explained previously, the fairly large magnetic anisotropy barrier must be attributed to the Fe ions. However, the Fe ions have a low spin of $S=1/2$, and so the single-ion anisotropy obtained from exact diagonalization of Eq. (7) apparently vanishes for the Fe ions. The only way to retrieve the barrier is via spin-orbit-coupling induced orbital angular momentum which may be

TABLE VI. Total spin S, the smallest HOMO-LUMO gap, the expectation value of the induced orbital angular momentum, and magnetic anisotropy barrier (MAB) for the four isolated parts of the three cyanide-bridged molecular magnets. See the text for the definition of the two values in the MAB.

	$[Tp\mathrm{Fe(CN)_3}]^{-1}$	$\mathrm{Mn}(\mu\text{-NC})_2(\mathrm{DMF})_4$	$\mathrm{Co}(\mu\text{-NC})_2(\mathrm{DMF})_4$	$\mathrm{Ni}(\mu\text{-NC})_2(\mathrm{DMF})_4$
Type	Easy axis	Easy axis	Easy plane	Easy plane
Total spin S	1/2	5/2	3/2	1
Energy gap (eV)	0.34	1.34	0.50	1.34
$\langle L\rangle_{\max}$	0.13	0.002	0.23	0.12
$\langle L\rangle_{\max}-\langle L\rangle_{\min}$	0.11	0.0009	0.11	0.02
MAB (K)	0, 12	0.2, 0.14	17, 17.2	2.2, 2.1

appreciable for the Fe ions given the ligand fields. The barrier caused by the induced orbital angular momentum for each Fe ion is calculated to be 12 K. The procedure of calculation is described in this and the next paragraphs. Near the Fermi level, the t_{2g} levels corresponding to the Fe ions in $[\mathrm{Fe}_2M_2]^{2+}$ (M=Mn,Co,Ni) are well split into three (except for the majority Fe $3d$ orbitals for $[\mathrm{Fe}_2\mathrm{Co}_2]^{2+}$ as illustrated in Fig. 3). The calculated gaps between these adjacent split levels are approximately 1306, 490, and 3265 K for $[\mathrm{Fe}_2M_2]^{2+}$ (M=Mn,Co,Ni). These splittings are large enough to expect partial or fully unquenched orbital angular momentum without spin-orbit coupling. We compute the expectation value of the induced orbital angular momentum with respect to the complex number of eigenvectors of the total Hamiltonian, $\mathcal{H}_{\mathrm{KS}}+\mathcal{H}_{\mathrm{SO}}^{1-\mathrm{el}}$, using the following formula: $|\langle\vec{L}\rangle| = \sqrt{\langle L_x\rangle^2+\langle L_y\rangle^2+\langle L_z\rangle^2}$. Henceforth, we simply write $|\langle\vec{L}\rangle|$ as $\langle L\rangle$. We find that the maximum values of the calculated spin-orbit-coupling induced $\langle L\rangle$ for the three molecular magnets are 4–8 times larger than that for Mn_{12} as shown in Table IV. The calculated $\langle L\rangle$ values vary as a spin vector rotates. The difference between the maximum and minimum values of $\langle L\rangle$ with rotation is significant for all of the three molecular magnets. This indicates that a large orbital angular momentum is induced by spin-orbit coupling for the three molecular magnets and that the induced orbital angular momentum greatly affects the magnetic anisotropy.

To further examine the sources of the magnetic anisotropy and of the induced orbital angular momentum, we break down a whole geometry into four pieces and investigate the magnetic properties of each piece separately. Each isolated piece consists of one transition metal ion and its surrounding ligands taken from the original geometry. We take into account four isolated parts, for example, $[Tp^*\mathrm{Fe(CN)_3}]^{1-}$, $\mathrm{Mn}(\mu\text{-NC})_2(\mathrm{DMF})_4$, $\mathrm{Co}(\mu\text{-NC})_2(\mathrm{DMF})_4$, and $\mathrm{Ni}(\mu\text{-NC})_2(\mathrm{DMF})_4$. The geometry of $[Tp^*\mathrm{Fe(CN)_3}]^{1-}$ is taken from the $[\mathrm{Fe}_2\mathrm{Mn}_2]^{2+}$ molecule. Our calculations show that the first two isolated parts have an easy axis, while the last two are close to easy-plane systems. Except for $\mathrm{Mn}(\mu\text{-NC})_2(\mathrm{DMF})_4$ all of the three parts have significant spin-orbit-coupling induced orbital angular momenta or strong spin-orbit coupling as shown in Table VI. However, as indicated in the case of $\mathrm{Ni}(\mu\text{-NC})_2(\mathrm{DMF})_4$, a strong spin-orbit coupling (or large induced orbital angular momentum) does not always guarantee a large magnetic anisotropy. Notice that the first number in the magnetic anisotropy (the last row of Table VI) for $[Tp^*\mathrm{Fe(CN)_3}]^{1-}$ is identical to zero because this is obtained by the exact diagonalization of the effective spin Hamiltonian, Eq. (7), in which $S=1/2$. However, the barrier obtained from the third method is 12 K for $[Tp^*\mathrm{Fe(CN)_3}]^{1-}$. In this case, the barrier obtained from the third method is more relevant for the magnetic anisotropy for $[\mathrm{Fe}_2\mathrm{Mn}_2]^{2+}$ because of the following reasons: (1) the total spin of $[\mathrm{Fe}_2\mathrm{Mn}_2]^{2+}$ is larger than $S=1/2$ and (2) the total magnetic anisotropy for the molecule is calculated by the anisotropy or angular dependence of the sum of the induced orbital angular momenta from the isolated parts, $[Tp^*\mathrm{Fe(CN)_3}]^{1-}$ and $\mathrm{Mn}(\mu\text{-NC})_2(\mathrm{DMF})_4$. For the $[\mathrm{Fe}_2\mathrm{Mn}_2]^{2+}$ molecule, the total magnetic anisotropy barrier or ($\langle L\rangle_{\max}-\langle L\rangle_{\min}$) amounts to approximately 2 times as large as that for $[Tp^*\mathrm{Fe(CN)_3}]^{1-}$ (Tables IV and VI). In the $[\mathrm{Fe}_2\mathrm{Co}_2]^{2+}$ and $[\mathrm{Fe}_2\mathrm{Ni}_2]^{2+}$ molecules, the magnetic anisotropy for $\mathrm{Co}(\mu\text{-NC})_2(\mathrm{DMF})_4$ and $\mathrm{Ni}(\mu\text{-NC})_2(\mathrm{DMF})_4$ *counteracts* that for $[Tp^*\mathrm{Fe(CN)_3}]^{1-}$. This is due to the fact that $\mathrm{Co}(\mu\text{-NC})_2(\mathrm{DMF})_4$ and $\mathrm{Ni}(\mu\text{-NC})_2(\mathrm{DMF})_4$ possess an easy plane, while $[Tp^*\mathrm{Fe(CN)_3}]^{1-}$ has an easy axis aligned perpendicular to the easy plane. Since the magnetic anisotropy for $\mathrm{Co}(\mu\text{-NC})_2(\mathrm{DMF})_4$ is comparable to that for $[Tp^*\mathrm{Fe(CN)_3}]^{1-}$, the total barrier for the $[\mathrm{Fe}_2\mathrm{Co}_2]^{2+}$ molecule is greatly reduced. Furthermore, the Ni ions have small magnetic anisotropy relative to the Co ions. This results in a smaller deduction from the Ni ions in the total anisotropy for the $[\mathrm{Fe}_2\mathrm{Ni}_2]^{2+}$ molecule. Thus, $[\mathrm{Fe}_2\mathrm{Co}_2]^{2+}$ has a much lower energy barrier to reverse its magnetic moment than $[\mathrm{Fe}_2\mathrm{Mn}_2]^{2+}$ and $[\mathrm{Fe}_2\mathrm{Ni}_2]^{2+}$.

The trend that the DFT-calculated magnetic anisotropy barrier for $[\mathrm{Fe}_2\mathrm{Co}_2]^{2+}$ is much smaller than that for $[\mathrm{Fe}_2\mathrm{Ni}_2]^{2+}$ agrees with experiment, although the DFT-calculated barriers for both $[\mathrm{Fe}_2\mathrm{Co}_2]^{2+}$ and $[\mathrm{Fe}_2\mathrm{Ni}_2]^{2+}$ tend to be lower than the experimentally deduced values. If the Fe ions did not contribute to the anisotropy barriers, the $\mathrm{Fe}_2\mathrm{Co}_2$ molecule would have a higher barrier than the $\mathrm{Fe}_2\mathrm{Ni}_2$ molecule because of the larger contributions of the Co ions to the total anisotropy than the Ni ions. Unlike the well-split t_{2g} levels of the Fe ions, the corresponding levels of the Mn, Co, and Ni ions are not well separated. The splitting of the Co t_{2g} levels in $[\mathrm{Fe}_2\mathrm{Co}_2]^{2+}$ is about 196 K. This small splitting compared to that for the Fe ions indicates that for the Co ions the orbital angular momentum would be substantially unquenched without spin-orbit coupling. For more quantitative

comparison to experiment, this effect must be included in the magnetic anisotropy unlike the other two cyanide-based molecular magnets. The experiment on the Fe_2Mn_2 molecule revealed a frequency-*independent* ac susceptibility above 1.8 K, which indicates the molecule does not behave as an SMM above 1.8 K, even though Fe_2Co_2 and Fe_2Ni_2 showed a SMM behavior. This experimental result remains an open question because the DFT calculation on $[Fe_2Mn_2]^{2+}$ suggested a fairly large magnetic anisotropy. One possible explanation is that there may exist contributions of higher-order transverse anisotropy terms and/or antisymmetric exchange terms to the spin Hamiltonian such as a Dzyaloshinsky-Moriya interaction.[49,50] These contributions would enhance the magnetic quantum tunneling such that a SMM behavior may be overshadowed even with a substantial magnetic anisotropy barrier. An example of this kind was recently reported for one type of Ni_4 SMMs.[51,52] In addition, for the $[Fe_2Mn_2]^{2+}$ molecule, the exchange constant J is much smaller than the magnetic anisotropy barrier as shown in Table IV. As a result, different spin multiplets become highly mixed and a total spin S is not a good quantum number. This would also make the measurement of the barrier difficult.

V. CONCLUSION

The electronic and magnetic properties of the three types of cyanide-bridged molecular magnets were studied with consideration of the single-electron spin-orbit interaction in DFT. The calculations on the exchange constants using broken-symmetry spin configurations revealed that in the ground state the metal ions in Fe_2Mn_2 are antiferromagnetically coupled, while those in Fe_2Co_2 and Fe_2Ni_2 are ferromagnetically coupled. For the three molecular magnets, a considerable amount of orbital angular momentum was induced by spin-orbit coupling and it contributed significantly to the magnetic anisotropy. However, in general, a strong spin-orbit coupling or a large induced orbital angular momentum does not necessarily lead to a large magnetic anisotropy barrier, as shown in the isolated part of the Fe_2Ni_2 molecule, $Ni(\mu\text{-}NC)_2(DMF)_4$. The calculated magnetic anisotropy originated mainly from the spin-orbit interaction within individual transition metal sites, neither from mixing terms between different metal sites, nor from spin-other-orbit coupling terms, Eq. (4), that were not included in the present DFT calculations. The first argument is corroborated by reasonable agreement between the total anisotropy barrier of each compound and the sum of the barriers of its constituents (Tables IV and VI). For example, the total barrier for the $[Fe_2Mn_2]^{2+}$ molecule is 22–26 K, while the barrier of $[Tp^*Fe(CN)_3]^{1-}$ is 12 K. The calculated total anisotropy barrier for $[Fe_2Co_2]^{2+}$ was much smaller than that for $[Fe_2Ni_2]^{2+}$ since the significant anisotropy of the Co ions counteracted the Fe ion contributions. The result obtained in this study may be used to explain an order of magnitude of the magnetic anisotropy barrier for a similar trinuclear system, $[(pzTp)Fe^{III}(CN)_3]_2[Ni^{II}(bipy)_2]$,[33] in which the angle formed by the first Fe ion, the Ni ion, and the second Fe ion is about 90 degrees. This trinuclear system was reported to behave as a SMM and the measured barrier was 20.6 K.[33] The Jahn-Teller effect is not expected for the local environment around the Ni ion and the single Ni ion anisotropy computed with an isolated part of the $[Fe_2Ni_2]^{2+}$ molecule showed no significant magnetic anisotropy. Therefore, the total anisotropy can be mainly determined by the anisotropy of the two Fe ions. As a result, our present study suggests that the total anisotropy barrier for the trinuclear system should be in the range of 20–26 K (refer to Table IV). The theoretical anisotropy barriers for $[Fe_2Co_2]^{2+}$ and $[Fe_2Ni_2]^{2+}$ tend to be underestimated compared to experimental values because of the following two reasons. First, DFT does not take into account low-energy excited spin multiplets in the calculation of spin-orbit coupling. According to the recent studies by Neese,[16] the effect of those excited spin multiplets amounted to about 50% of the total barrier for some SMMs. Second, the calculated anisotropy terms are attributed to the spin-orbit-coupling induced orbital angular momentum only, neither from partially unquenched orbital angular momentum without spin-orbit coupling nor from purely orbital anisotropy. In contrast to the experimental finding of frequency-independent ac magnetic susceptibility for Fe_2Mn_2, we found the substantial magnetic anisotropy for the molecule caused by the anisotropy in the induced orbital angular momentum of the Fe ions. Several plausible sources of significant transverse anisotropy terms would mask the effect of the anisotropy barrier in Fe_2Mn_2. However, it still remains an open question why Fe_2Mn_2 has not shown a SMM behavior although it has a similar structure as Fe_2Co_2 and Fe_2Ni_2.

ACKNOWLEDGMENTS

This work was partially supported by the Terascale Computing Facility at Virginia Tech and by the National Center for Supercomputing Applications under Grant No. DMR060009N and utilized the NCSA SGI Altix and NCSA Xeon Linux Supercluster. One of the authors (K.P.) is thankful to Gordon T. Yee and Mark R. Pederson for stimulating discussions and to Tunna Baruah for allowing usage of an unpublished part of the NRLMOL that she wrote. One of the authors (S.M.H.) is grateful to the National Science Foundation (Grant No. MRI CHE-0319176) and to the Kentucky Science and Engineering Foundation (Grant Nos. KSEF-621-RDE-006 and KSEF-0992-RDE-008) for financial support.

*Electronic address: kyungwha@vt.edu
†Electronic address: smholm2@uky.edu

[1] J. R. Friedman, M. P. Sarachik, J. Tejada, and R. Ziolo, Phys. Rev. Lett. **76**, 3830 (1996).
[2] A. L. Barra, D. Gatteschi, and R. Sessoli, Phys. Rev. B **56**, 8192 (1997).
[3] S. Hill, J. A. A. J. Perenboom, N. S. Dalal, T. Hathaway, T. Stalcup, and J. S. Brooks, Phys. Rev. Lett. **80**, 2453 (1998); J. A. A. J. Perenboom, J. S. Brooks, S. Hill, T. Hathaway, and N. S. Dalal, Phys. Rev. B **58**, 330 (1998).
[4] E. M. Chudnovsky and J. Tejada, *Macroscopic Quantum Tunneling of the Magnetic Moment*, Cambridge Studies in Magnetism Vol. 4 (Cambridge University Press, Cambridge, 1998).
[5] T. Lis, Acta Crystallogr., Sect. B: Struct. Sci. **36**, 2042 (1980).
[6] M. R. Pederson and S. N. Khanna, Phys. Rev. B **60**, 9566 (1999).
[7] W. Kohn and L. J. Sham, Phys. Rev. **140**, A1133 (1965).
[8] K. Park, M. A. Novotny, N. S. Dalal, S. Hill, and P. A. Rikvold, Phys. Rev. B **65**, 014426 (2002).
[9] S. Hill, S. Maccagnano, K. Park, R. M. Achey, J. M. North, and N. S. Dalal, Phys. Rev. B **65**, 224410 (2002).
[10] M. Hennion, L. Pardi, I. Mirebeau, E. Suard, R. Sessoli, and A. Caneschi, Phys. Rev. B **56**, 8819 (1997).
[11] I. Mirebeau, M. Hennion, H. Casalta, H. Andres, H. U. Güdel, A. V. Irodova, and A. Caneschi, Phys. Rev. Lett. **83**, 628 (1999).
[12] G. Chaboussant, A. Sieber, S. Ochsenbein, H.-U. Güdel, M. Murrie, A. Honecker, N. Fukushima, and B. Normand, Phys. Rev. B **70**, 104422 (2004).
[13] M. Dressel, B. Gorshunov, K. Rajagopal, S. Vongtragool, and A. A. Mukhin, Phys. Rev. B **67**, 060405(R) (2003).
[14] K. Park, M. R. Pederson, S. L. Richardson, N. Aliaga-Alcalde, and G. Christou, Phys. Rev. B **68**, 020405(R) (2003).
[15] W. Wernsdorfer, N. Allaga-Alcalde, D. N. Hendrickson, and G. Christou, Nature (London) **416**, 406 (2002).
[16] F. Neese, J. Am. Chem. Soc. **128**, 10213 (2006).
[17] J. Kortus, C. S. Hellberg, and M. R. Pederson, Phys. Rev. Lett. **86**, 3400 (2001).
[18] K. Park, M. R. Pederson, and N. Bernstein, J. Phys. Chem. Solids **65**, 805 (2004).
[19] K. Park, M. R. Pederson, and C. S. Hellberg, Phys. Rev. B **69**, 014416 (2004).
[20] T. Baruah, J. Kortus, M. R. Pederson, R. Wesolowski, J. T. Haraldsen, J. L. Musfeldt, J. M. North, D. Zipse, and N. S. Dalal, Phys. Rev. B **70**, 214410 (2004).
[21] A. V. Postnikov, M. Bruger, and J. Schnack, Phase Transitions **78**, 47 (2005).
[22] E. Fermi and E. Amaldi, Accad. Ital. Rome **6**, 119 (1934).
[23] J. P. Perdew and A. Zunger, Phys. Rev. B **23**, 5048 (1981).
[24] R. A. Heaton, J. G. Harrison, and C. C. Lin, Phys. Rev. B **28**, 5992 (1983); M. R. Pederson, R. A. Heaton, and C. C. Lin, J. Chem. Phys. **80**, 1972 (1984); M. R. Pederson and C. C. Lin, *ibid.* **88**, 1807 (1988).
[25] D. W. Boukhvalov, A. I. Lichtenstein, V. V. Dobrovitski, M. I. Katsnelson, B. N. Harmon, V. V. Mazurenko, and V. I. Anisimov, Phys. Rev. B **65**, 184435 (2002).
[26] D. W. Boukhvalov, V. V. Dobrovitski, M. I. Katsnelson, A. I. Lichtenstein, B. N. Harmon, and P. Kögerler, Phys. Rev. B **70**, 054417 (2004).
[27] J. J. Sokol, A. G. Hee, and J. R. Long, J. Am. Chem. Soc. **124**, 7656 (2002).
[28] C. P. Berlinguette, D. Vaughn, C. Canada-Vilalta, J. R. Galan-Mascaros, and K. R. Dunbar, Angew. Chem., Int. Ed. **42**, 1523 (2003).
[29] E. J. Schelter, A. V. Prosvirin, and K. R. Dunbar, J. Am. Chem. Soc. **126**, 15004 (2006).
[30] H. J. Choi, J. J. Sokol, and J. R. Long, Inorg. Chem. **43**, 1606 (2004).
[31] S. Wang, J. L. Zuo, H. C. Zhou, H. J. Choi, Y. X. Ke, J. R. Long, and X. Z. You, Angew. Chem., Int. Ed. **43**, 5940 (2004).
[32] D. Li, S. Parkin, G. B. Wang, G. T. Yee, A. V. Prosvirin, and S. M. Holmes, Inorg. Chem. **44**, 4903 (2005).
[33] D. Li, R. Clerac, S. Parkin, G. B. Wang, G. T. Yee, and S. M. Holmes, Inorg. Chem. **45**, 5251 (2006).
[34] D. Li, S. Parkin, G. Wang, G. T. Yee, R. Clérac, W. Wernsdorfer, amd S. M. Holmes, J. Am. Chem. Soc. **128**, 4214 (2006).
[35] Y. Q. Zhang, C. L. Luo, and Z. Yu, New J. Chem. **29**, 1285 (2005).
[36] L. M. Toma, R. Lescouezec, J. Pasan, C. Ruiz-Perez, J. Vaissermann, J. Cano, R. Carrasco, W. Wernsdorfer, F. Lloret, and M. Julve, J. Am. Chem. Soc. **128**, 4842 (2006).
[37] P. Albores, L. D. Slep, T. Weyhermuller, E. Rentschler, and L. M. Baraldo, Dalton Trans. **7**, 948 (2006).
[38] A. V. Palii, S. M. Ostrovsky, S. I. Klokishner, B. S. Tsukerblat, C. P. Berlinguette, K. R. Dunbar, and J. R. Galan-Mascaros, J. Am. Chem. Soc. **126**, 16860 (2004).
[39] B. S. Tsukerblat, A. V. Palii, S. M. Ostrovsky, S. V. Kunitsky, S. I. Klokishner, and K. R. Dunbar, J. Chem. Theory Comput. **1**, 668 (2005).
[40] M. R. Pederson and K. A. Jackson, Phys. Rev. B **41**, 7453 (1990); K. A. Jackson and M. R. Pederson, *ibid.* **42**, 3276 (1990); D. V. Porezag, Ph.D. thesis, Chemnitz Technical Institute, 1997.
[41] J. P. Perdew, K. Burke, and M. Ernzerhof, Phys. Rev. Lett. **77**, 3865 (1996).
[42] D. Porezag and M. R. Pederson, Phys. Rev. A **60**, 2840 (1999).
[43] K. Park, E.-C. Yang, and D. N. Hendrickson, J. Appl. Phys. **97**, 10M522 (2005).
[44] R. S. Edwards, S. Maccagnano, E. C. Yang, S. Hill, W. Wernsdorfer, D. Hendrickson, and G. Christou, J. Appl. Phys. **93**, 7807 (2003).
[45] J. P. Perdew and Y. Wang, Phys. Rev. B **45**, 13244 (1992).
[46] K. Park and M. R. Pederson, Phys. Rev. B **70**, 054414 (2004).
[47] R. Boča, *Theoretical Foundations of Molecular Magnetism* (Elsevier Science S.A., Lausanne, 1999).
[48] M. R. Pederson and T. Baruah (unpublished).
[49] I. Dzyaloshinski, J. Phys. Chem. Solids **4**, 241 (1958).
[50] T. Moriya, Phys. Rev. Lett. **4**, 228 (1960); Phys. Rev. **120**, 91 (1960).
[51] A. Sieber, C. Boskovic, R. Bircher, O. Waldmann, S. T. Ochsenbein, G. Chaboussant, H. U. Gudel, N. Kirchner, J. van Slageren, W. Wernsdorfer, A. Neels, H. Stoeckli-Evans, S. Janssen, F. Juranyi, and H. Mutka, Inorg. Chem. **44**, 4315 (2005).
[52] N. Kirchner, Ph.D. thesis, Physikalisches Institut, Universität Stuttgart, 2006.